Linearity Characteristics of GaAs HBTs and the Influence of Collector Design

Masaya Iwamoto, *Student Member, IEEE*, Peter M. Asbeck, *Fellow, IEEE*, Thomas S. Low, Craig P. Hutchinson, Jonathan Brereton Scott, *Senior Member, IEEE*, Alex Cognata, Xiaohui Qin, Lovell H. Camnitz, *Member, IEEE*, and Donald C. D'Avanzo, *Member, IEEE*

***Abstract*—Linearity characteristics of GaAs heterojunction bipolar transistors (HBTs) are studied through measurement and analysis. Third-order intermodulation distortion behavior of HBTs is examined on devices with various epilayer designs and at various bias points, loads, and frequencies. Calculations from an analytical model reveal a strong bias and load dependence of third-order intercept point (IP3) on the nonlinearities from transconductance and the voltage dependence of base-collector capacitance. However, a simple model is not able to predict the fine details of IP3 with bias. A large-signal HBT model with an accurate description of the base-collector charge is shown to account for the measured trends. The base-collector charge function accounts for the modulation of base-collector capacitance with current, electron velocity modulation, and Kirk effect (base pushout) for GaAs-based HBTs. A detailed study of the influence of collector design on linearity is also presented.**

***Index Terms*—Heterojunction bipolar transistors (HBTs), intermodulation distortion, nonlinear distortion, semiconductor device modeling.**

I. Introduction

GaAs-BASED heterojunction bipolar transistors (HBTs) have recently found widespread application in radio-frequency (RF)/microwave power amplifiers. With their high-frequency performance and power-handling capabilities, HBTs are attractive active devices for transmitters in RF/microwave communication applications. An important requirement for such devices is to have acceptable distortion characteristics, or linearity. The power level of spurious frequencies generated by intermodulation of the in-band signals is an important measure of device linearity. Linearity characterizations of GaAs and InP-based HBTs have shown excellent results in adjacent channel power ratio (ACPR) and third-order intercept point (IP3) [1]–[3].

There have been numerous studies on the intermodulation distortion behavior of HBTs through both analysis and measurement. From these works, it is evident that there are two major distortion components in HBTs: transconductance (g_m) and base-collector capacitance (C_{BC}). There have been several papers that have investigated the internal cancellation effect of nonlinear currents utilizing Volterra series. Analysis in [4] showed that the nonlinear currents from the resistive and reactive parts of the nonlinear base-emitter junction partially cancelled. In the analyses of [5] and [6], it was shown that the total nonlinear currents generated by the base-emitter junction (I_E) and the base-collector junction (I_C, not including C_{BC}), partially cancelled. Among other effects, these works highlight the nonlinear currents caused by the nonlinear behavior of g_m. In [7], it was shown that the emitter and base resistances (R_E and R_B) linearize g_m through the well-known feedback effect.

The other major distortion source in HBTs is the nonlinearity of C_{BC} with voltage [3], [6]–[9]. Measurements have shown significant improvements in IP3 when V_{CE} is biased high enough to fully deplete, or punch-through, the collector [3], [6], [8]. These studies have suggested epilayer structures with a low collector punch-through voltage for highly linear performance at low voltages. A practical linearity figure of merit (LFOM), given by the ratio IP3/P_{DC}, considers both linearity and efficiency. According to this ratio, a lower V_{CE} with the same level of IP3 results in a high LFOM.

The linearity study for this paper begins in Section II with two-tone measurements on HBTs with variations on the emitter, base, and collector profiles. It is found that collector variations have the most effect on IP3. In Section III, the observations from these measurements are used to formulate a simple nonlinear analytical model using Volterra series. The aforementioned nonlinear current cancellation effect is also observed in this model. Subsequently in Section IV, calculations from this model are compared with measured results of IP3 as a function of current, voltage, load, and frequency. The model is able to predict the general trends from measurements and is used as a tool to explain the observed IP3 behavior. Analysis shows that g_m and C_{BC} nonlinearities are dominant in certain bias areas and loads. However, this model shows a significant deficiency in the detailed predictions of IP3 as a function of current. Motivated by this fact, the current dependence of IP3 is investigated further in Section V with measurements on HBTs with various collector profiles. Measurement results indicate a complex behavior of IP3 as a function of current with discernable maximas and minimas that are dependent on the collector profile. From simulations, it is shown that the modulation of C_{BC}, transit time, and electron velocity with current all have a significant impact on the linearity characteristics and that a large-signal HBT model, which includes the above-mentioned effects, is able to

Manuscript received March 6, 2000.

M. Iwamoto and P. M. Asbeck are with the Department of Electrical and Computer Engineering, University of California at San Diego, La Jolla, CA 92092 USA.

T. S. Low, C. P. Hutchinson, J. B. Scott, A. Cognata, X. Qin, and D. C. D'Avanzo are with the Microwave Technology Center, Agilent Technologies, Santa Rosa, CA 95403 USA.

L. H. Camnitz is with the Agilent Laboratories, Palo Alto, CA 94304 USA.

Publisher Item Identifier S 0018-9480(00)10732-X.

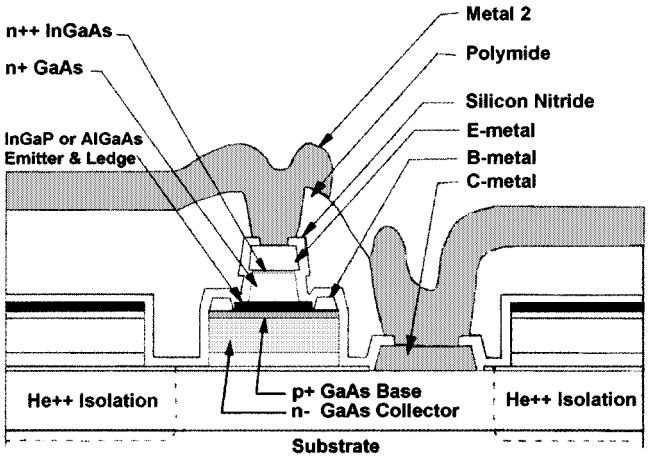

Fig. 1. Cross-section of InGaP and AlGaAs emitter HBTs.

predict the measured trends [10]. In general, it is found that most of the intermodulation distortion mechanisms of HBTs can be accounted for by the nonlinear behavior of the base–collector charge (Q_{BC}) together with the inevitable nonlinear g_m that is dominant in the low current regime.

II. Experimental Technique

A. Device Description

All devices characterized in this work are $2 \times 8\ \mu\text{m}^2$ emitter area GaAs-based HBTs. InGaP emitter HBTs are the primary focus in the study, but several AlGaAs emitter HBTs were examined for comparison purposes. Representative epilayer structures for both InGaP and AlGaAs emitter HBTs were selected, and designs that have slight variations from these devices were also chosen to identify the influence on linearity of epilayer parameter variations.

A cross section of the HBT for both the InGaP and AlGaAs emitter devices is shown in Fig. 1. The AlGaAs emitter process has a graded emitter, a nonalloyed n^+ InGaAs emitter contact, a nonalloyed base contacts, an alloyed collector contact, and a depleted passivation ledge. The InGaP emitter process is almost identical to the AlGaAs emitter process except for the substitution of an abrupt heterojunction InGaP emitter. A more detailed description of both processes is presented in [11] and [12]. It is also shown in these references that the InGaP emitter HBTs inherently possess high reliability at high current densities $(J_C \sim 0.6\ \text{mA}/\mu\text{m}^2)$: MTTF $> 5 \times 10^5$ h compared to $<8 \times 10^4$ hrs for the AlGaAs emitter process. Since power amplifiers are typically biased in the high current regime, InGaP emitter HBTs are excellent devices for this application. In Table I, selected device parameters are summarized for the two representative devices. The significant differences between the two devices are the material of the emitters and the base widths.

B. Measurement Approach

All of the measurements for this study were done on a load-pull system including three Agilent 83 650B sources and an Agilent 8510C network analyzer, which was used to measure vector corrected on-wafer power, large signal S_{11}, and Γ_L $(1/S_{22})$ of the two-tone $(f_1$ and $f_2)$ signals. An Agilent 8565E spectrum analyzer was used for measuring output power of the intermodulation products at the upper and lower sidebands. One of the sources was used as the dedicated 8510C system source to provide broadband calibration and the a_1 phase-lock signals during the measurement. The other two sources were locked to the 8510C system source by its 10-MHz reference oscillator and provided the f_1 and f_2 input stimulus. Load pull was implemented by either a Maury microwave passive tuner at lower frequencies (up to 2 GHz) or an active load at higher frequencies (above 2 GHz). The details of this measurement system are presented in [13] and [14].

Identical bias points and loads were chosen for all of the devices in order to have a consistent comparison. Class A bias was set at $V_{CE} = 2.7$ V, $J_C = 0.6\ \text{mA}/\mu\text{m}^2$ $(I_C = 9.6$ mA), and Γ_L of $0.647\angle{-3.3}^\circ$ $(Z_L = 230 - j30\ \Omega)$. Measurements were taken at 2 and 5 GHz. A 1-MHz tone spacing was carefully chosen as a compromise between the need to avoid low-frequency dispersion [15] and the risk of having a large difference in the load presented at the two-tone frequencies. Harmonic loading and source-pull were not implemented, and the source impedance was 50 Ω in all cases.

For two-tone linearity measurements, four parameters were measured: power gain, 1-dB compression point $(P_{1\,\text{dB}})$ per tone, third-order intermodulation products at $P_{1\,\text{dB}}$ $(\text{IM3}_{1\,\text{dB}})$ measured in dBc, and output IP3. Since power gain and IP3 are small-signal measurements, whereas $P_{1\,\text{dB}}$ and $\text{IM3}_{1\,\text{dB}}$ are large-signal measurements, power sweeps over a wide range (over 20 dB) were taken for each device. Although IP3 is calculated from a single point measurement, care was taken to make sure it was extrapolated in the "3:1 IM3 to fundamental power ratio" regime.

C. Summary of Measurements with Varying Epilayer Designs

Table II summarizes the linearity measurements of the HBTs with variations on the epilayer structures. Two emitter variations of the AlGaAs emitter HBT were chosen for measurements. As seen in Table II, they have lower and higher emitter dopings. The effects of varying the doping are apparent, where by lowering the doping, a lower gain and higher IP3 are observed. Increasing the doping yields exactly the opposite results. This can be explained in simple terms by the emitter doping's influence on R_E. R_E is dependent on g_{mx}, the extrinsic transconductance, by the relationship

$$g_{mx} = \frac{g_m}{1 + g_m(R_E + R_B/\beta)} \tag{1}$$

where β is the dc current gain and g_m is the intrinsic transconductance given by the expression

$$g_m = \frac{\partial I_C}{\partial V_{BE}} = \frac{qI_C}{kT} \tag{2}$$

and I_C is the collector current. It is related in a nonlinear fashion to input voltage by

$$I_C = I_S\left(\exp\left(\frac{qV_{BE}}{\eta kT}\right) - 1\right). \tag{3}$$

TABLE I
SELECTED DEVICE PARAMETERS OF REPRESENTATIVE HBTs

	W_C (Å)	W_B (Å)	R_E (Ω)	R_B (Ω)	β @J_C=0.6mA/μm^2	f_t (GHz) @J_C=0.6mA/μm^2 & V_{CE}=1.5V
InGaP emitter	4000	800	3.4	24.4	113	61
AlGaAs emitter	4000	600	6.9	32.6	102	63

TABLE II
HBT LINEARITY DATA OF VARIOUS EPILAYER DESIGNS

(♦=InGaP emitter; •=AlGaAs emitter)

Description	Gain (dB)	P_{1dB} (dBm)	$IM3_{1dB}$ (dBc)	IP3 (dBm)	Gain (dB)	P_{1dB} (dBm)	$IM3_{1dB}$ (dBc)	IP3 (dBm)	
(♦) InGaP emitter	27.5	5.0	-23.6	20.6	21.1	5.1	-25.1	21.3	representative devices
(•) AlGaAs emitter	25.5	5.0	-23.1	22.1	19.4	5.3	-23.1	22.3	
(•) lower doped emitter (R_E=7.9Ω)	24.9	4.8	-24.2	23.2	18.9	5.1	-23.7	22.8	emitter variations
(•) higher doped emitter (R_E=2.8Ω)	27.3	5.0	-24.4	21.0	20.7	5.2	-24.2	20.5	
(♦) thinner base (W_B=600Å)	27.7	4.9	-24.5	20.3	21.0	4.9	-25.6	21.3	base variation
(♦) longer collector (W_C=8000Å)	28.4	1.8	-25.1	14.0	22.0	0.5	-25.1	11.8	collector variations
(♦) longer collector (W_C=11000Å)	27.6	1.2	-24.5	13.2	21.0	-0.4	-23.5	10.6	
	f_o=2GHz				f_o=5GHz				

When I_C is increased, g_{mx} approaches the value

$$g_{mx} \approx \frac{1}{(R_E + R_B/\beta)} \tag{4}$$

which is independent of current, and thereby linear. Since $\beta \cdot R_E$ is usually larger than R_B, g_{mx} is determined predominantly by R_E in the high current region. Although increasing R_E linearizes g_{mx}, R_E also lowers its magnitude and causes a decrease in the power gain.

The base variation was a reduction in the thickness. Table II shows that decreasing the base width does not result in a significant change in either IP3 or gain. This observation is consistent with simulation predictions in [6].

Finally, the collector variations are considered. The principle variation was to increase the collector thickness with a slightly lower collector doping. It is apparent in Table II that this has a significant influence on IP3. The decrease in IP3 can be attributed to the nonlinearity of C_{BC} as a function of V_{CE} [6]. A plot of C_{BC} versus V_{CE} with $V_{BE} = 0$ V in Fig. 2 clearly shows that the 8000-Å collector has a more nonlinear C_{BC} than the 4000-Å collector at a V_{CE} of 2.7 V. Previous studies have demonstrated that biasing the collector of the HBT in the fully depleted region, or the constant C_{BC} region, results in the highest IP3 [3], [6], [8]. This explanation is valid at certain bias regions, and a detailed examination in Section V will further elaborate on the influence of collector design.

Results from Table II show that third-order intermodulation distortion of HBTs in the small-signal region (characterized by IP3) is significantly dependent on the emitter doping and collector profile. A distinction can be made between mechanisms for strong and weak nonlinearities. Strong nonlinearities arise from the consequences of a large-signal swing, which include saturation and cutoff of the HBT as well as interactions between higher order intermodulation currents. Weak nonlinearities arise from the weakly nonlinear behavior of conductances and capacitances and can be analytically calculated by a small-signal model. The primary focus of this study is to understand the intermodulation distortion mechanisms of HBTs in the weak regime by both measurements and analysis, and therefore IP3 is extensively used as a measure of device linearity.

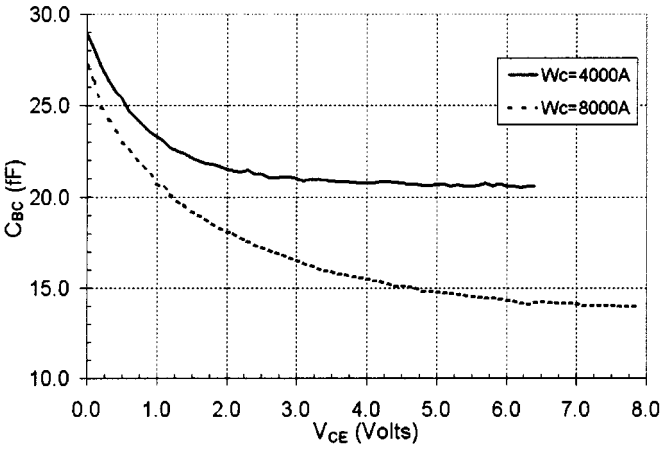

Fig. 2. Measured C_{BC} versus V_{CE} (with $V_{BE} = 0$ V) for 4000- and 8000-Å collector profiles.

III. SIMPLIFIED MODEL FOR NONLINEAR ANALYSIS

In this section, a small-signal analytical model with nonlinear elements is formulated as a tool to understand IP3 behavior. Since similar methods of analysis for HBTs have been previously presented in detail [4]–[6], only a brief description of the derivation will be presented. From the results in the preceding section and previous representative linearity studies of HBTs [3]–[9] and Si bipolar junction transistors (BJTs) [16]–[18], it is apparent that nonlinearities from g_m and C_{BC} have a significant influence on intermodulation distortion. Therefore, el-

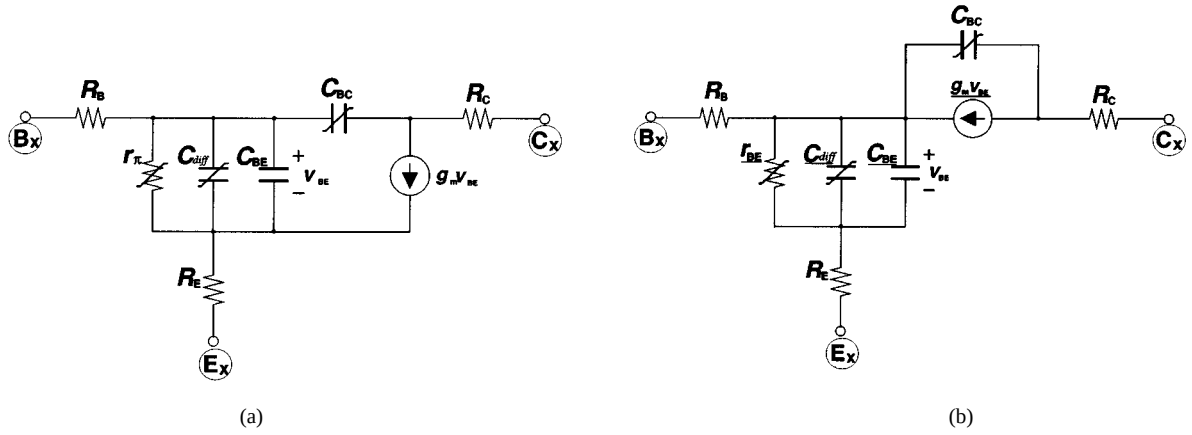

Fig. 3. HBT small-signal model with nonlinear elements: (a) standard hybrid-π model and (b) model used for nonlinear analysis.

ements that are related to these parameters are modeled using nonlinear analysis.

A. Derivation of the Simplified Model

The fundamental small-signal model is the hybrid-π model shown in Fig. 3(a). The nonlinear components in the analysis are $C_{BC}, r_\pi, C_{\text{diff}}$, and the voltage-controlled current source (VCCS) $g_m V_{BE}$. Here, r_π is the nonlinear junction resistance defined by β/g_m and C_{diff} is the diffusion capacitance given by $g_m\tau$, where τ is the transit time. The analysis assumes a common-emitter configuration, where the input and output correspond to the base and collector, respectively, with the emitter grounded. Although this model appears simple, it is rather difficult to analyze because of the shunt feedback from C_{BC} and the series feedback due to R_E. The analysis can be somewhat simplified by splitting the VCCS from the collector node to the base node and from the base node to the emitter node, and it can be further simplified by combining r_π and the VCCS across the base and emitter nodes, as shown in Fig. 3(b). This combined resistance r_{BE} is equal to the value α/g_m, where α is the common base current gain. This derived model resembles the T-model of the bipolar transistor.

The nonlinear elements are r_{BE}, C_{diff}, the VCCS, and C_{BC}. Volterra series "method of nonlinear currents" [19] is used to calculate the nonlinear current contributions. This nonlinear analysis method is appropriate for IP3 calculations since all of the distortion components are weak nonlinearities.

For simplification, the standard Gummel–Poon model expression for C_{BC} as a function of bias is used in the analysis. More sophisticated expressions, which include the full depletion of the collector and the current dependence, can be found in [20] and [21]. The capacitance equation can be approximated by the expansion

$$C_{BC} = \frac{C_{JC}}{\left(1 - \dfrac{v_{BC}}{V_{JC}}\right)^{MJC}} \approx c_0 + c_1 v_{BC} + c_2 v_{BC}^2 \tag{5}$$

where c_1 and c_2 are coefficients related to the first and second derivatives of C_{BC} with respect to voltage, respectively.

The voltage across the internal base and collector nodes is defined in terms of "orders" of voltages given by

$$v_{BC} = v_{BC1} + v_{BC2} + v_{BC3} + \cdots \tag{6}$$

where v_{BC1} and v_{BC2} represent the first-order (f_1 and f_2 frequencies) and second-order ($2f_2$ and f_2-f_1 frequencies, for example) voltages, respectively, and so on. The total current from C_{BC} is given by the expression

$$i_{Cbc} = C_{BC}\frac{\partial v_{BC}}{\partial t} \tag{7}$$

and, solving for the nonlinear current terms relevant to the third-order intermodulation frequencies

$$i_{Cbc(2f_1-f_2,2f_2-f_1)} = c_1\left(v_{BC2}\frac{\partial v_{BC1}}{\partial t} + v_{BC1}\frac{\partial v_{BC2}}{\partial t}\right) + c_2 v_{BC1}^2\frac{\partial v_{BC1}}{\partial t}. \tag{8}$$

This nonlinear current expression generated by C_{BC} indicates that both the first and second derivatives of C_{BC} with respect to v_{BC} are important.

Nonlinear g_m currents can be calculated in a similar fashion. g_m nonlinearities are described by the current–voltage relationship:

$$i_C \approx g_0 + g_1 v_{BE} + g_2 v_{BE}^2 + g_3 v_{BE}^3. \tag{9}$$

The voltage across the internal base and emitter nodes can be expressed in terms of "orders" of voltages given by

$$v_{BE} = v_{BE1} + v_{BE2} + v_{BE3} + \cdots. \tag{10}$$

All three nonlinear elements associated with g_m (VCCS, r_{BE}, and C_{diff}) are related to the current generated by g_m given by the general expression

$$i_{gm} = A g_m v_{BE} \tag{11}$$

where A is 1 for the VCCS, $1/\alpha$ for r_{BE}, and $j\omega\tau$ for C_{diff}. Solving for the nonlinear current terms pertinent to the IM3 frequencies yields

$$i_{gm_{(2f_1-f_2,2f_2-f_1)}} = A(2g_2 v_{BE1} v_{BE2} + g_3 v_{BE1}^3). \tag{12}$$

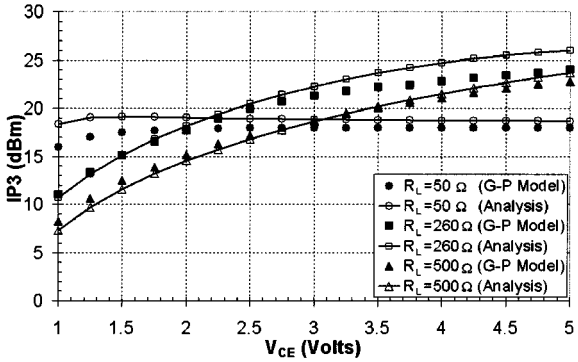

Fig. 4. Comparison of calculations using the simple analytical model and an equivalent Gummel–Poon large-signal model with harmonic balance simulations.

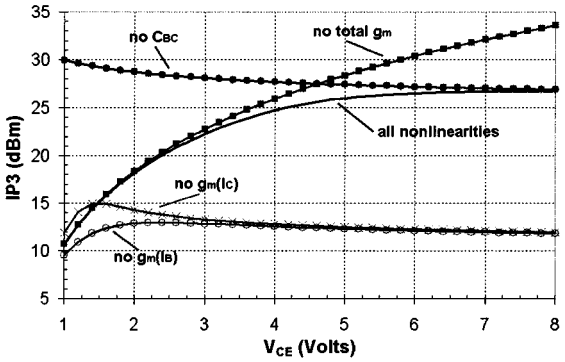

Fig. 5. Calculated IP3 versus V_{CE} with specific nonlinear components removed. ($J_C = 0.6$ mA/μm^2 and $R_L = 260\ \Omega$.

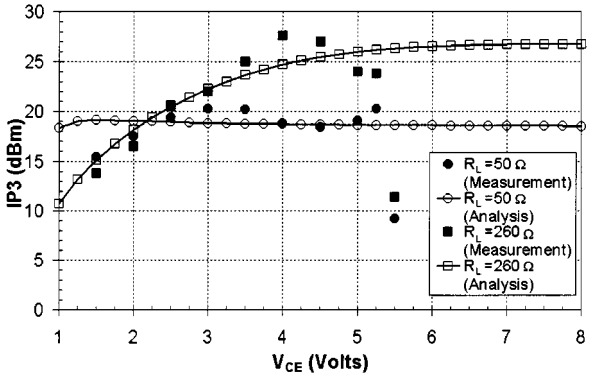

Fig. 6. IP3 versus V_{CE}: measurements and calculations at $J_C = 0.6$ mA/μm^2.

Finally, the total IM3 current through the load is calculated from the above current expressions [notably (8) and (12)] and the linear circuit in Fig. 3(b). The source impedance is set to 50 Ω, and the load impedance is a user-definable parameter. Loads presented to the harmonics as well as the difference frequencies are not separately specified and are assumed to be the same as the load at the fundamental. It is well known that varying the load presented to these frequencies is important [5], but harmonic loading is not part of the linearity study for this particular work.

All of the equations are implemented in and solved by MATLAB. To verify the accuracy of this simple nonlinear analytical model, simulation results were compared to harmonic balance simulations with an equivalent Gummel–Poon large signal model using Agilent Microwave Design System (MDS). Fig. 4 shows that the simple analytical model is able to predict the IP3 simulation trends of the more sophisticated large-signal model.

B. Contribution of Individual Nonlinear Sources

The analytical model can be used to examine the influence of the nonlinear elements to intermodulation distortion. Since the linear circuit is solved independently of the nonlinear circuit, specific nonlinearities can be removed without affecting the linear response of the circuit. As an example, a plot of IP3 versus V_{CE} illustrates the nonlinear current contributions. For simplification, five cases are examined:

1) all nonlinearities;
2) no C_{BC} nonlinearities;
3) no total g_m nonlinearties;
4) no g_m nonlinearities from the base-emitter junction ($g_m(I_B)$ currents);
5) no g_m nonlinearities from the base-collector junction ($g_m(I_C)$ currents).

Fig. 5 shows the results for the five cases.

When no C_{BC} nonlinearities are present, a significant improvement in IP3 is observed in the low V_{CE} region. This is consistent with the influence of the nonlinear voltage dependence of C_{BC} in (5). When total g_m nonlinearities are excluded, improvements in IP3 are observed in the higher V_{CE} regime. When only one of the g_m nonlinear currents from either the base-emitter or base-collector junctions is removed, a drastically lower level of IP3 is observed. As explained in [5] and [6], and also by the model, the reason for the higher IP3 levels when all g_m currents are present rather than only one is due to the fact that g_m currents from the two junctions partially cancel.

IV. Influence of Bias, Load, and Frequency

The bias, load, and frequency dependencies of IP3 were measured with the representative InGaP emitter HBTs as described in Section II. A similar study for Si BJTs has been presented by Narayanan [16]. The parameters of the analytical model in Section III were fit to the characteristics of the measured devices. Since the mode of operation assumes a common-emitter configuration in the forward active region, only a few parameters were necessary for the model. Some key parameters include the parasitic resistances, C_{BC} as a function of voltage, f_t at peak value, and the saturation current density I_S.

A. Influence of Bias Voltage

IP3 was measured as a function of voltage with two different loads $R_L = 50\ \Omega$ ($\Gamma_L = 0$) and $R_L = 260\ \Omega$ ($\Gamma_L = 0.68$). The current was set at $J_C = 0.6$ mA/μm^2 ($I_C = 9.6$ mA), and the two-tone frequencies were at 5 GHz with a 1-MHz spacing. The measurement results are shown with calculated predictions in Fig. 6.

The behavior of IP3 versus voltage is strikingly different with different loads. For 50 Ω, the analytical model shows that distortion across V_{CE} is dominated by g_m nonlinearities. This ex-

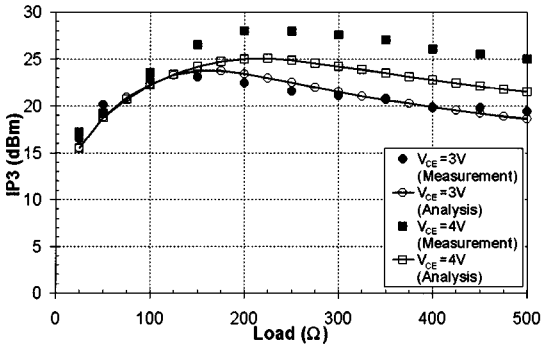

Fig. 7. IP3 versus output load: measurements and calculations at $J_C = 0.6$ mA/μm^2.

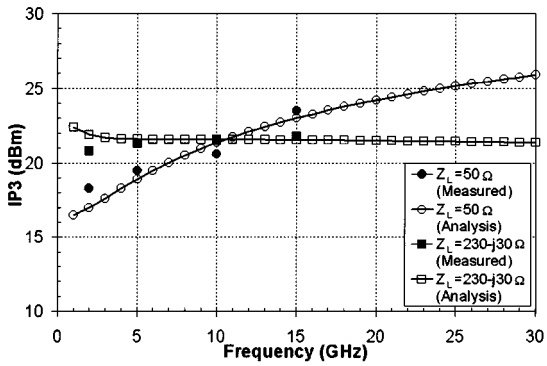

Fig. 8. IP3 versus frequency: measurements and calculations at $V_{CE} = 2.7$ V and $J_C = 0.6$ mA/μm^2.

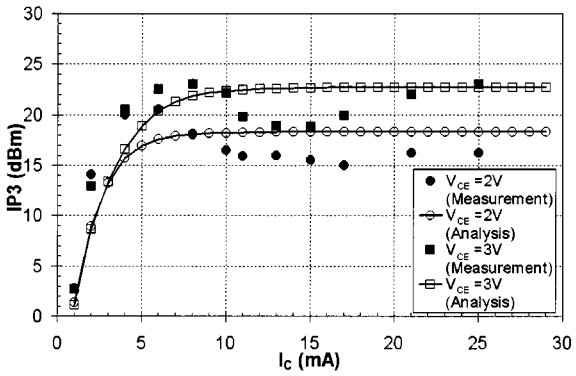

Fig. 9. IP3 versus I_C: Measurements and calculations with $R_L = 260\ \Omega$.

plains the flat IP3 behavior as a function of voltage in the calculations since nonlinear g_m currents are not strongly influenced by V_{CE}. The measurements, however, only show this flat trend in the region of V_{CE} between 2.5 and 5 V. Low IP3 at the highest V_{CE} can be explained by distortion due to breakdown effects, which is not implemented in the model. The measured decrease in IP3 below 2.5 V is due to the nonlinearities from Kirk effect, which are also not implemented in the model (explained more in detail in Section V). For 260 Ω, there is a significant voltage dependence of IP3. The analytical model shows that at low voltages, distortion contribution from C_{BC} is dominant and IP3 improves as the voltage is increased. This directly corresponds to a decrease in the nonlinearities from C_{BC} as the base-collector junction is reverse biased ($W_C = 4000$ Å device in Fig. 2). The highest IP3 is measured when the collector is "punch throughed," which is consistent with results from [6], [8], and [9]. C_{BC} nonlinearities are prominent at 260 Ω and not at 50 Ω because of the magnitude of the voltage swing across C_{BC}. The analytical model shows that larger loads entail larger voltage swings across C_{BC} and thus more nonlinear contribution from this capacitance.

B. Influence of Load

The impedance presented to the output of the device was varied to investigate its influence on IP3. The load was kept nearly real, i.e., minimal output reactance, so the effect of the magnitude of load on IP3 could be studied. Fig. 7 shows measured IP3 versus load for V_{CE} of 3 and 4 V at a center frequency of 5 GHz, spacing of 1 MHz, and $J_C = 0.6$ mA/μm^2.

The analytical model shows that there are distinct regions where g_m and C_{BC} nonlinearities dominate. At smaller loads, IP3 is determined by g_m nonlinearties and the power gain. This is also suggested by the fact that IP3 is not strongly dependent on V_{CE} in the measurements. As the load is increased, the analytical model shows that g_m nonlinearity decreases and power gain increases, and results in an improvement in IP3. At higher loads, C_{BC} nonlinearities dominate. This is supported by the fact that IP3 levels are different at the two V_{CE} biases in both measurements and calculations. The analytical model shows that the gradual decrease in IP3 at higher loads is due to the increasing nonlinear current contribution from C_{BC} [16]. The large differences between measurements and calculations at $V_{CE} = 4$ V in the higher load region are likely due to the fact that the full depletion of the collector is not modeled in the C_{BC} equation of (5). The analytical model shows that the peak in IP3 is due to a transition between the g_m and C_{BC} dominant regions.

C. Influence of Frequency

Fig. 8 shows IP3 versus frequency with 1-MHz tone spacing at two loads (50 Ω and 230 $j30\ \Omega$) measured at $V_{CE} = 2.7$ V and $J_C = 0.6$ mA/μm^2. The variation of IP3 with frequency depends significantly on the output load. At smaller loads (50 Ω), both measurements and calculations show an improvement as the frequency is increased. Since g_m nonlinearities are the dominant source of distortion at this load and bias point in the analytical model, the improvement in IP3 is due to a decrease in g_m nonlinearities as the frequency is increased. The improvement is not solely due to the stray emitter inductance since the analytical model does not include this element. When C_{BC} nonlinearities are dominant ($Z_L = 230 - j30\ \Omega$, there is very little variation in IP3 as the frequency is increased for both measurements and calculations. Although IP3 stays nearly constant, IM3 level generally decreases since the power gain decreases.

D. Influence of Bias Current

IP3 was measured as a function of current at $V_{CE} = 2$ V and $V_{CE} = 3$ V. The two-tone frequencies were set again at 5 GHz with spacing of 1 MHz, and the load was set to $R_L = 260\ \Omega$. Fig. 9 shows measured results with calculated predictions.

The analytical model shows that g_m nonlinearities dominate at low currents. Since g_m nonlinearites are weakly dependent on

TABLE III
COLLECTOR PROFILES AND SELECTED CHARACTERISTICS OF THE THREE HBTs IN SECTION V

	N_C (cm^{-3})	W_C (Å)	BV_{ceo} (V)	V_{pt} (V)	J_{crit} (mA/μm²)	f_t at J_{crit} (GHz)
HBT-A	$2.7x10^{16}$	4000	8.1	2.5	0.91	60
HBT-B	$1.5x10^{16}$	5000	10.0	1.5	0.62	56
HBT-C	$0.9x10^{16}$	7000	13.6	1.5	0.42	47

V_{CE} in the model, this explains the similar values of IP3 at the two V_{CE} biases. It should also be noted that power gain is less at lower currents due to a smaller g_m, which in turn influences IP3. As the current is increased, g_m nonlinearities are decreased due to R_E and R_B, and eventually, distortion from C_{BC} nonlinearties dominates. In the measurements and calculations, the level of IP3 is higher at $V_{CE} = 3$ V than at $V_{CE} = 2$ V in the C_{BC} dominant region. However, it is evident that the analytical model is not able to accurately predict the trends in IP3 in this region. This is because the model does not account for transit time and C_{BC} nonlinearities due to Kirk effect. In Section V, these additional nonlinearities will be investigated, and it will be shown that the "dip" in IP3 roughly corresponds to the Kirk effect condition.

V. INFLUENCE OF COLLECTOR DESIGN

It was shown in Section II that the variations in the collector profile had a significant effect on IP3. Furthermore, it was shown in Section IV that modeling the bias dependence of C_{BC} with only V_{BC} was not sufficient to predict IP3, especially as a function of current. Previous works on HBT linearity have stressed the importance of optimizing the collector profile [6], [8], [9]. An extensive simulation study for Si BJTs has also suggested optimizing the collector profile [18]. Since current modulates the collector space-charge, it is meaningful to examine the linearity characteristics as a function of collector current.

A. Characterization of Collector Design Variations

Three InGaP emitter devices with significantly different collector dopings (N_C) and widths (W_C) were selected for characterization. The epilayers of the HBTs (HBT-A, HBT-B, HBT-C) are identical above the base. HBT-A (identical to the "representative InGaP device" in Section II) has a base width of 800 Å, while HBT-B and HBT-C have base widths of 600 Å. The different base widths should not have a significant influence on IP3, as was shown in Section II. The layout of these devices is slightly different from the ones studied in the previous sections, where these three devices employ a single base-finger layout. A separate study (which is not presented here) was done on the linearity differences between a single- and a double-base contact layout. It was found that there were no significantly large differences in IP3, which is consistent with observations from [7]. Table III summarizes the collector profiles and characteristics of the three devices.

The differences in collector doping and thickness result in breakdown voltage variations. In the first-order approximation, the breakdown voltage can be increased by reducing N_C and increasing W_C. From Table III, it is evident that improving the breakdown voltage in this manner lowers $J_{\rm crit}$, where $J_{\rm crit}$ is defined as the critical current density at which f_t peaks. This roughly corresponds to the onset of the Kirk effect condition. $J_{\rm crit}$ can be analytically calculated if it is approximated as $J_{\rm crit0}$, the current density at which the carrier concentration equals the doping concentration and the electric field at the base-collector junction is reduced to zero. $J_{\rm crit0}$ is given by the expression

$$J_{\rm crit0} = v_s \left(qN_C + \frac{2\varepsilon_s(V_{CB} + V_{bi})}{W_C^2} \right) \approx J_{\rm crit} \qquad (13)$$

where q is the electron charge, v_s is the electron velocity, ε_s is the permitivity, and V_{bi} is the built-in potential of the junction. Since the peaking of f_t is typically observed above the current when the field at the base-collector junction reaches zero, $J_{\rm crit}$ will be slightly higher than $J_{\rm crit0}$.

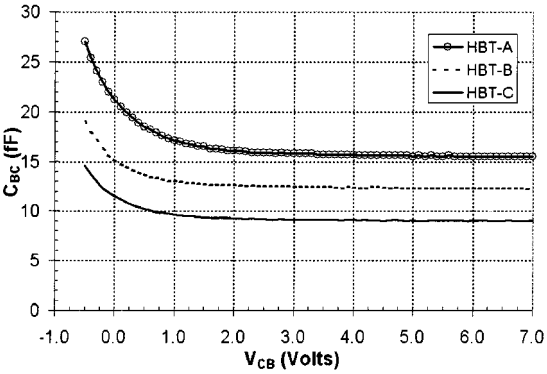

Fig. 10. Measured C_{BC} versus V_{CB} of HBT-A, HBT-B, and HBT-C with $V_{BE} = 0$ V.

Fig. 10 shows C_{BC} as a function of V_{CB} with $V_{BE} = 0$ V, illustrating that C_{BC} (with no collector current) becomes a constant at a relatively low V_{pt}. V_{pt} is defined from measurements as the voltage at which C_{BC} becomes nearly a constant minimum value. This corresponds to the condition when the collector depletion layer reaches the subcollector with an appropriate reverse bias voltage. V_{pt} can be analytically estimated using the depletion and one-sided abrupt junction approximations

$$V_{pt} = \frac{qW_C^2 N_C}{2\varepsilon_s} - V_{bi}. \qquad (14)$$

Fig. 11(a) shows IP3 as a function of current density at a fixed load ($R_L = 260\ \Omega$), frequency ($f_o = 5$ GHz with 1 MHz tone spacing), and bias voltage. V_{CE} is biased high enough to ensure the collector is fully depleted (HBT-A = 4 V, HBT-B = 5 V, HBT-C = 5 V). The general trends are consistent for all three devices, and show there are significant peaks and troughs in the IP3 behavior. However, the values of IP3 and current densities at which these peaks and troughs occur are dependent on the collector design. As Fig. 11(b) shows, $J_{\rm crit}$ corresponds to the current density at the trough that occurs after the peak in IP3. The peak always appears at a current density slightly lower than $J_{\rm crit}$. Furthermore, a higher value of $J_{\rm crit}$ generally results in higher levels of IP3.

Fig. 12(a) and (b) shows plots of IP3 as a function of V_{CE} at 0.3 mA/μm^2 (4.8 mA) and 0.6 mA/μm^2 (9.6 mA), respectively. The general improvement in IP3 for increasing V_{CE} is

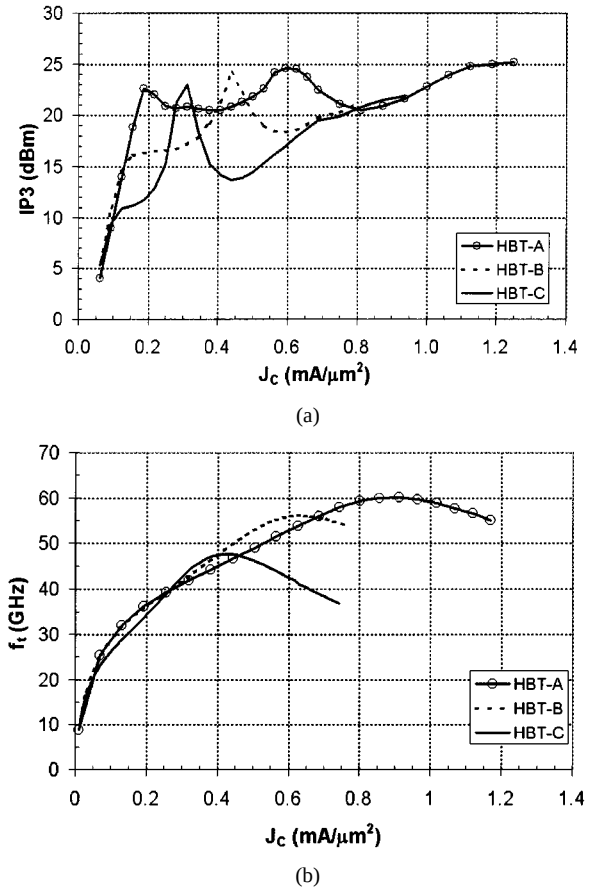

Fig. 11. (a) Measured IP3 versus J_C and (b) measured f_t versus J_C. (HBT-A: $V_{CE} = 4$ V; HBT-B and HBT-C: $V_{CE} = 5$ V).

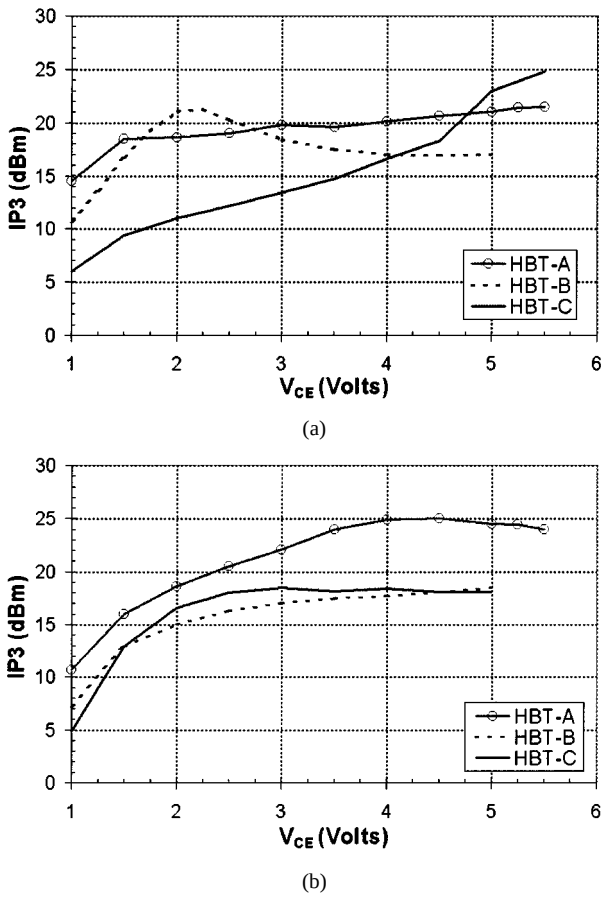

Fig. 12. Measured IP3 versus V_{CE} at (a) $J_C = 0.3$ mA/μm^2 and (b) $J_C = 0.6$ mA/μm^2.

again attributed to the fact that C_{BC} becomes less nonlinear as the base-collector junction is reverse biased. Fig. 12(b) clearly shows that IP3 reaches a plateau when V_{CE} is biased beyond V_{pt} at $J_C = 0.6$ mA/μm^2. However, IP3 does not level off at the same value of IP3 for different collector designs. Moreover, at $J_C = 0.3$ mA/μm^2 (in Fig. 12(a)), IP3 does not always plateau when V_{CE} is biased beyond V_{pt}. These observations suggest that there are sources of distortion other than the nonlinear voltage dependence of C_{BC}. The IP3 versus V_{CE} characteristics at $J_C = 0.3$ mA/μm^2 can be explained by examining a plot of both IP3 and f_t as a function of J_C of HBT-C in Fig. 13. At $J_C = 0.3$ mA/μm^2 and $V_{CE} = 5$ V, IP3 for this device is at the sharp peak in the plot of IP3 versus J_C. As was previously shown, this peak and the subsequent trough are related to the value of J_{crit}. Since J_{crit} is dependent on V_{CE} according to (13), the position in current of the peak in IP3 should decrease when V_{CE} is decreased. Fig. 13 shows the locations of the peaks and troughs of IP3 when V_{CE} is biased at 2 and 5 V. A slight change in V_{CE} from the 5-V bias point will significantly change the value in IP3 due to the sharp peak. The sudden increase in IP3 of 7 dB in Fig. 12(a) between $V_{CE} = 4.5$ and 5.5 V is due to this effect. It should be noted that the collector is fully depleted in this voltage range, and therefore the nonlinearities from the voltage dependence of C_{BC} are at a minimum. It is then evident that Kirk effect has a significant influence on the linearity characteristics even at bias points beyond V_{pt} and below J_{crit}. Fig. 14 shows a dc I–V plot of HBT-C. Also plotted are values

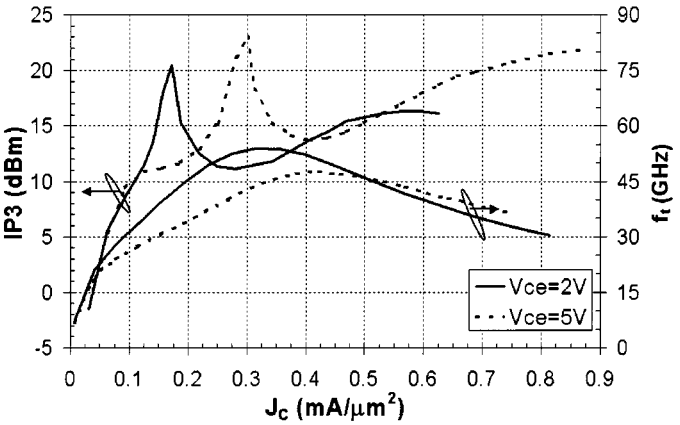

Fig. 13. Measured IP3 and f_t versus J_C of HBT-C at $V_{CE} = 2$ and 5 V.

of J_{crit} at different V_{CE} (denoting the onset of Kirk effect). The figure shows that Kirk effect has little influence on the dc characteristics [22]. The "overshoot" of IP3 observed for HBT-B in Fig. 12(a) is also due to the voltage dependence of J_{crit}. In this case, the peak in IP3 [in Fig. 11(a)] decreases in current as V_{CE} is decreased, and "crosses" $J_C = 0.3$ mA/μm^2 at a V_{CE} of 2.2 V.

The measurement results indicate Kirk effect and the full depletion of the collector (quantified by J_{crit} and V_{pt}, respectively) are important mechanisms that influence linearity characteristics of HBTs. Since the characteristics of these two effects are

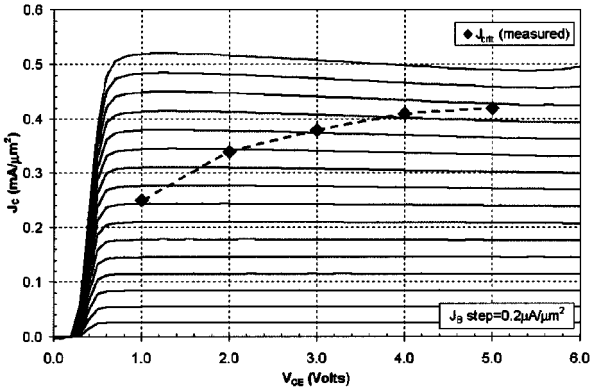

Fig. 14. Collector current density versus collector voltage characteristics of HBT-C with measured $J_{\rm crit}$.

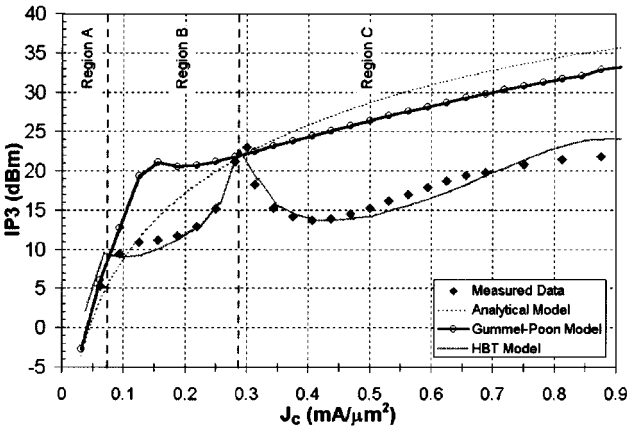

Fig. 15. HBT-C: Measured and simulated IP3 versus J_C.

determined by the collector thickness and doping, designing an HBT with linear performance requires a careful selection of the collector profile.

B. Analysis of Collector Design

A standard Gummel–Poon (GP) model and an HBT model based on [21] were extracted to compare with the observed linearity behavior. DC and S-parameter data were acquired using an Agilent 4142 DC source/monitor and 8510C network analyzer both controlled by Agilent IC-CAP modeling software, and model parameter fits were done using MDS. The HBT model is implemented as a symbolically defined device in MDS. The model topology resembles that of the GP model but differs in the definitions of the junction charge functions. The charge functions model the high-frequency behavior of the device, particularly the capacitances and delay time effects. Some salient features of the model are the following.

1) The intrinsic base-collector charge function is defined by the equation

$$Q_{BC} = \frac{CJC \cdot VJC}{1-MJC} \cdot \left|1 - \frac{I_C}{qcc \cdot ICRITO}\right|^{MJC} \cdot \left(1 - \frac{V_{BC}}{VJC}\right)^{(1-MJC)} + \frac{TFCO \cdot I_C}{qcc} \quad (15)$$

where the first term models the bias dependence of the collector depletion layer as functions of both voltage and current. The definitions for CJC, MJC, and VJC are identical to the GP model, and $ICRIT0$ is given by $qA_EN_Cv_s$ [similar to the bias-independent part of (13)]. This equation is only valid below V_{pt}. When the collector is fully depleted, the charge function switches to

$$Q_{BC} = CCMIN \cdot \left[(V_{BC} - VJC) + \left(\frac{VJC \cdot MJC}{(MJC-1)}\right) \cdot \left|1 - \frac{I_C}{qcc \cdot ICRITO}\right| \cdot \left(\frac{CJC}{CCMIN}\right)^{1/MJC}\right] + \frac{TFCO \cdot I_C}{qcc} \quad (16)$$

where $CCMIN$ represents C_{BC} at the collector punch-through condition.

2) Electron velocity modulation for the GaAs collector material is modeled by the parameter qcc in (15) and (16)

$$qcc = \frac{(I + (I_C/ITC)^2)}{[1 + (VJC - V_{BC})/VTC + (I_C/ITC2)^3]} \quad (17)$$

where VTC accounts for the increase in collector transit time (τ_C) with an increase in V_{BC} and ITC models the decrease in τ_C as I_C is increased. $ITC2$ terminates the contribution of ITC at high currents. The model is able to take into account the effect of τ_C varying with bias even with a fixed collector depletion layer width.

3) Kirk effect is implemented by the charge function

$$Q_{krk} = TKRK \cdot I_C \cdot e^{((V_{BC}/VKRK)+(I_C/IKRK))}. \quad (18)$$

To expedite simulation time, the thermal subcircuit in [21] was excluded. It is worthwhile to mention that the equations for the base-collector and base-emitter charge functions are similar to the equations utilized in the DARPA/UCSD HBT model.[1]

Harmonic balance simulations based on the two large-signal models are compared with the measured IP3 versus J_C results in Fig. 11(a) for HBT-C. Fig. 15 shows this plot at $V_{CE} = 5$ V with calculated predictions from the analytical model (fit to HBT-C) presented in Section III. While the GP model and the analytical model do not predict the strong variation of IP3 with current, the HBT model shows excellent agreement with measured trends.

Parameters of the HBT model were varied in order to provide insight into the complex behavior of IP3 as a function of current. At low currents (exemplified by region A in Fig. 15), distortion is dominated by the nonlinear contributions from g_m and improves as current is increased. All three models exhibit this trend.

As the current is increased further, other mechanisms begin to dominate. The HBT model shows that the nonlinear relationship between base–collector charge (Q_{BC}) and J_C controls IP3. For example, in region B of Fig. 15 (current densities below the peak in IP3), the detailed values of $ICRIT0$ and qcc govern the behavior of IP3. Simulations show that the magnitude of $\delta C_{BC}/\delta J_C$ has a strong influence on IP3 in this region. From a physical standpoint, in this region the charge in the collector depletion region varies with both I_C and V_{CE}. Also, the effective

[1]See http://hbt.ucsd.edu.

electron velocity changes as a function of the electric field in the collector. The influence of this velocity modulation is complex and can lead, for example, to "capacitance cancellation," for which it is possible for C_{BC} to decrease with current even when the collector is biased beyond V_{pt} [22].

At the highest current density (region C in Fig. 15), distortion due to Kirk effect begins to dominate. The peak in IP3 occurs at the transition between regions B and C. There are two major sources of distortion from Kirk effect. One is the nonlinearity of the electron transit time, which is related to the diffusion charge. Nonlinearity from this parameter is discernable in a plot of f_t versus J_C and is dominant in the vicinity of $J_{\rm crit}$. In keeping with this, for the various collector designs, the breadth of the f_t versus J_C peaks resembles the breadth of the IP3 versus J_C troughs in Fig. 11(a) and (b). Furthermore, from qualitative observations, the curvature at the f_t peak appears to be related to the value of IP3 at $J_{\rm crit}$, where smaller curvature results in higher IP3. These observations are consistent with distortion analysis for Si BJTs on the influence of f_t on distortion [23]. The other source of distortion from Kirk effect is the increase in C_{BC} due to a decrease in the effective width of the collector depletion region. The influence of this nonlinearity is evident at the highest currents where IP3 levels off.

Although the explanation of the current dependence of IP3 is based on simulations of an empirical HBT model, it is evident that collector space-charge effects have a significant role in determining the linearity characteristics of HBTs. Therefore, a large-signal HBT model should accurately account for these effects when it is used for distortion simulations.

VI. Conclusions

Third-order intermodulation distortion characteristics of GaAs heterojunction bipolar transistors were examined in detail. Measurements on devices with various emitter, base, and collector profiles showed that the collector variations had the most significant influence on intermodulation behavior. A simple analytical nonlinear HBT model was presented and used to explain observations from measurements with various biases, loads, and frequencies. The analytical model showed that there were certain bias and load conditions where g_m and C_{BC} nonlinearties dominate.

The influence of collector design on the intermodulation distortion behavior was studied in detail. Measurement of IP3 as a function of current was observed to be complex. A local minimum appears in IP3 at the critical current density for Kirk effect, $J_{\rm crit}$. A large-signal HBT model that includes effects such as the modulation of C_{BC} with current, Kirk effect, and velocity modulation was able to predict the complex behavior of IP3 with current. For accurate distortion predictions, a large-signal model should include the description of collector space-charge effects that are specific to the collector material of the HBT.

Acknowledgment

The authors would like to thank D. Root, T. Shirley, and D. Hornbuckle of Agilent Technologies and Mani Vaidyanathan, L. Larson, and P. Yu of the University of California, San Diego, for technical discussions concerning this research. They would also like to thank J. Wood, J. Tra, and D. Davis at Agilent Technologies for measurement and software support.

References

[1] T. Iwai, S. Ohara, H. Yamada, Y. Yamaguchi, K. Imanishi, and K. Joshin, "High efficiency and high linearity InGaP/GaAs HBT power amplifiers: Matching techniques of source and load impedance to improve phase distortion and linearity," *IEEE Trans. Electron Devices*, vol. 45, pp. 1196–1200, June 1998.

[2] B. L. Nelson, D. K. Umemoto, C. B. Perry, R. Dixit, B. R. Allen, M. E. Kim, and A. K. Oki, "High-linearity, low DC power monolithic GaAs HBT broadband amplifiers to 11 GHz," in *Proc. 1990 IEEE MMWMC Symp.*, pp. 15–18.

[3] K. W. Kobayashi, J. C. Cowles, L. T. Tran, A. Gutierrez-Aitken, M. Nishimoto, J. H. Elliot, T. R. Block, A. K. Oki, and D. C. Streit, "A 44–GHz high IP3 InP HBT MMIC amplifier for low dc power millimeter-wave receiver applications," *IEEE J. Solid-State Circuits*, vol. 34, pp. 1188–95, Sept. 1999.

[4] S. A. Mass, B. L. Nelson, and D. L. Tait, "Intermodulation in heterojunction bipolar transistors," *IEEE Trans. Microwave Theory Tech.*, vol. 40, pp. 442–448, Mar. 1992.

[5] A. Samelis and D. Pavlidis, "Mechanisms determining third-order intermodulation distortion in AlGaAs/GaAs HBTs," *IEEE Trans. Microwave Theory Tech.*, vol. 40, pp. 2374–2380, Dec. 1992.

[6] J. Lee, W. Kim, Y. Kim, T. Rho, and B. Kim, "Intermodulation mechanism and linearization of AlGaAs/GaAs HBTs," *IEEE Trans. Microwave Theory Tech.*, vol. 45, pp. 2065–2072, Dec. 1997.

[7] N. L. Wang, W. J. Ho, and J. A. Higgins, "AlGaAs/GaAs HBT linearity characteristics," *IEEE Trans. Microwave Theory Tech.*, vol. 42, pp. 1845–1850, Oct. 1994.

[8] K. W. Kobayashi, A. K. Oki, J. C. Cowles, L. T. Tran, P. C. Grossman, T. R. Block, and D. C. Streit, "The voltage-dependent IP3 performance of a 35–GHz InAlAs/InGaAs-InP HBT amplifier," *IEEE Microwave Guided Wave Lett.*, vol. 7, pp. 66–68, Mar. 1997.

[9] D. Teeter, M. Karakucuk, J. East, and G. Haddad, "Analysis of intermodulation in GaAs/AlGaAs HBTs," in *1992 MTT-S Dig.*, June 1992, pp. 263–266.

[10] M. Iwamoto, T. S. Low, C. P. Hutchinson, J. B. Scott, A. Cognata, X-H. Qin, L. H. Camnitz, P. M. Asbeck, and D. C. D'Avanzo, "Influence of collector design on InGaP/GaAs HBT linearity," in *IEEE MTT-S Int. Microwave Symp. Dig.*, June 2000.

[11] T. S. Low, T. S. Shirley, C. P. Hutchinson, G. K. Essilfie, W. C. Whiteley, R. E. Yeats, and D. C. D'Avanzo, "InGaP HBT Technology for RF and Microwave Instrumentation," *Solid-State Electron.*, vol. 43, pp. 1437–1444, Aug. 1999.

[12] T. S. Low, C. P. Hutchinson, P. C. Canfield, T. S. Shirley, R. E. Yeats, J. S. C. Chang, G. K. Essilfie, M. K. Culver, W. C. Whiteley, D. C. D'Avanzo, N. Pan, J. Elliot, and C. Lutz, "Migration from an AlGaAs to an InGaP emitter HBT IC process for improved reliability," in *GaAs IC Symp. Tech. Dig.*, 1998, pp. 153–156.

[13] B. Hughes, A. Ferrero, and A. Cognata, "Accurate on-wafer power and harmonic measurements of mm-wave amplifiers and devices," in *IEEE MTT-S Int. Microwave Symp. Dig.*, June 1992, pp. 1019–1022.

[14] M. Demmler, B. Hughes, and A. Cognata, "A 0.5-50 GHz on-wafer, intermodulation, load-pull and power measurement system," in *IEEE MTT-S Int. Microwave Symp. Dig.*, May 1995, pp. 1041–1044.

[15] K. Lu, P. M. McIntosh, C. M. Snowden, and R. D. Pollard, "Low-frequency dispersion and its influence on the intermodulation performance of AlGaAs/GaAs HBTs," in *IEEE MTT-S Int. Microwave Symp. Dig.*, 1996, pp. 1373–76.

[16] S. Narayanan, "Transistor distortion analysis using Volterra series representation," *Bell Syst. Tech. J.*, vol. 46, no. 3, pp. 991–1024, May/June 1967.

[17] H. F. F. Jos, "A model for the nonlinear base-collector depletion layer charge and its influence on intermodulation distortion in bipolar transistors," *Solid-State Electron.*, vol. 33, no. 7, pp. 907–915, 1990.

[18] L. C. N. de Vreede, H. C. de Graff, J. A. Willemen, W. van Noort, R. Jos, L. E. Larson, J. W. Slotboom, and J. L. Tauritz, "Bipolar transistor epilayer design using the MAIDS mixed-level simulator," *IEEE J. Solid-State Circuits*, vol. 34, pp. 1331–1337, Sept. 1999.

[19] S. A. Maas, *Nonlinear Microwave Circuits*. Norwood, MA: Artech House, 1988, pp. 190–199.

[20] P. C. Grossman and J. Choma, Jr., "Large-signal modeling of HBT's including self-heating and transit time effects," *IEEE Trans. Microwave Theory Tech.*, vol. 40, pp. 449–464, Mar. 1992.

[21] L. H. Camnitz, S. Kofol, T. S. Low, and S. R. Bahl, "An accurate, large signal, high frequency model for GaAs HBTs," in *GaAs IC Symp. Tech. Dig.*, 1996, pp. 303–306.
[22] L. H. Camnitz and N. Moll, "An analysis of the cutoff-frequency behavior of microwave heterostructure bipolar transistors," in *Compound Semiconductor Transistors, Physics and Technology*. New York: IEEE Press, 1993, pp. 21–46.
[23] H. C. Poon, "Implication of transistor frequency dependence on intermodulation distortion," *IEEE Trans. Electron Devices*, vol. ED-21, Jan. 1974.

Masaya Iwamoto (S'99) received the B.S. degree from Cornell University, Ithaca, NY, in 1997 and the M.S. degree from the University of California at San Diego (UCSD) in 1999, both in electrical engineering. He is currently pursuing the Ph.D. degree at UCSD.

His research interests include HBT device characterization and power amplifier design. During the summers of 1997–2000, he was an Intern at Agilent Technologies (formerly Hewlett-Packard), Santa Rosa, CA.

Mr. Iwamoto received the Honarable Mention Award for his paper at the 2000 International Microwave Symposium Student Paper Competition concerning the topic of HBT linearity.

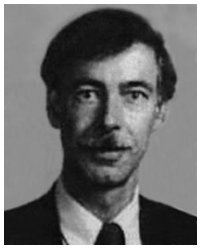

Peter M. Asbeck (M'75–SM'97–F'00) received the B.S. and Ph.D. degrees from the Electrical Engineering Department, Massachusetts Institute of Technology, Cambridge, in 1969 and 1975, respectively.

He worked at the Sarnoff Research Center, Princeton, NJ, and Philips Laboratory, Briarcliff Manor, NY, in the areas of quantum electronics and GaAlAs/GaAs laser physics and applications. In 1978, he joined Rockwell International Science Center, where he was involved in the development of high-speed devices and circuits based on III–V compounds and heterojunctions. He pioneered the effort to develop heterojunction bipolar transistors based on GaAlAs/GaAs and InAlAs/InGaAs materials and has contributed widely in the areas of physics, fabrication, and applications of these devices. In 1991, he joined the University of California at San Diego as a Professor in the Department of Electrical and Computer Engineering. His research interests are in development of high-speed heterojunction transistors and optoelectronic devices and their circuit applications. His research has led to more than 200 publications.

Dr. Asbeck is a Distinguished Lecturer of the IEEE Electron Device Society.

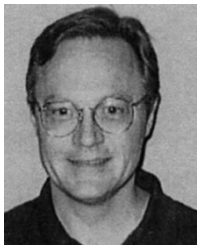

Thomas S. Low was born in Rockford, IL, in 1951. He received the B.S. degree from Purdue University, West Lafayette, IN, in 1975 and the M.S. and Ph.D. degrees from the University of Illinois, Urbana-Champaign, in 1978 and 1984, all in physics.

He was with Hewlett Packard Labs, Palo Alto, CA, until 1989, providing semiconductor characterization support to several epi rowth developments, including MOCVD and MBE PHEMTs, Be-doped AlGaAs HBTs, and InGaAs PIN photodetectors. In 1989, he joined Hewlett Packard's Microwave Technology Center, Santa Rosa, CA, to help with the transfer of HBT IC process and epigrowth technology to the manufacturing site, which culiminated in an InGaP HBT IC production release in 1998. He currently works at the same site for Agilent Technologies. His current interests include process design and device physical modeling of InGaP HBT ICs and various other optical and electronic heterojunction devices.

Craig P. Hutchinson received the B.S. degree in electrical engineering form the University of California, Davis, in 1984.

He joined Avantek in 1984, designing broadband GaAs integrated circuits, including, amplifiers, switches, and attenuators. He joined Pacific Monolithics in 1988, where he was responsible for the design of GaAs integrated circuits, including mixers, amplifiers, oscillators, and T/R modules. Since 1990, he has been with Avantek/Hewlett-Packard/Agilent Technologies, Santa Rosa, CA, designing high-speed silicon bipolar, GaAs MESFET, and, since 1996, GaAs HBT integrated circuits for Agilent's instrumentation product lines.

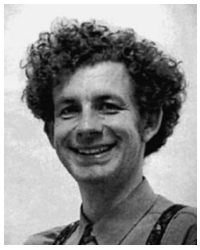

Jonathan Brereton Scott (M'82–SM'98) was born in Brisbane, Australia, in 1956. He received the B.Sc. and B.E. degrees from the University of Sydney, Sydney, Australia, in 1977 and 1979, respectively. He received the master of engineering science and Ph.D. degrees from Sydney University.

After working at the Air Navigation Group, a research arm of the Department of Transport, he worked on microwave transient digitization and gained . He was a Consultant in a variety of industries, including radar and analog signal processing. He was Manager of the Sydney Microwave Design Resource Centre from 1988 to 1992, as well as a Senior Lecturer in the Department of Electrical Engineering, University of Sydney. He was involved in establishing and subsequently teaching in the Graduate Program in Audio in the School of Architectural and Design Science. In 1995, he was a Visitor at University College, London, and subsequently a Visiting Lecturer at the University of Western Sydney. In 1994, he worked with Macquarie University on nonlinear electronic systems and helped set up the Collaborative Nonlinear Electronic Research Facility (CNERF) in conjunction with the Electronics Department at Macquarie University and Macquarie Research Ltd. In 1997, he became Chief Engineer at RF Technology Ltd. In 1999, he joined Hewlett-Packard, now Agilent Technologies, in the Microwave Technology Division, Santa Rosa, CA. He has served on committees of the Standards Association of Australia, is an Honorary Associate of Macquarie University, and is the author of more than 50 refereed publications and an undergraduate textbook.

Dr. Scott is a Fellow of the Institution of Engineers, Australia, and a member of the Audio Engineering Society. He received the Electrical Engineering Foundation medal for Excellence in Teaching in 1994. He received a British Telecom Research Fellowship in 1993.

Alex Cognata recieved the associate of science degree in electronic technology from Santa Rosa Junior College, Santa Rosa, CA, in 1983.

He is presently working at Agilent Technologies, Santa Rosa, developing measurement system hardware and software. He codeveloped a vector-corrected 45 MHz–50 GHz harmonic loadpull system with capabilities of measuring intermodulation distortion under tuned conditions. With this system, a wide variety of large-signal measurement capabilities are provided for model verification, FET/HBT process, and IC characterization.

Xiaohui Qin received the Ph.D. degree in electrical engineering from the University of California, Los Angeles, in 1995.

From 1995 to 1996, she was with Hughes Electronics as an MMIC Circuit Designer. In 1996, she joined the Microwave Technology Center, Hewlett-Packard Company (now Agilent Technologies), Santa Rosa, CA. Her research interests include active and passive component, packaging and interconnect modeling, and microwave and millimeter-wave subsystem design and development.

Lovell H. Camnitz (S'80–M'85) received the B.S.E.E. degree from Rensselaer Polytechnic Institute, Troy, NY, in 1980. He received the M.S.E.E. degree and the Ph.D. degree in electrical engineering from Cornell University, Ithaca, NY, in 1984 and 1986, respectively.

His graduate work was in the field of low noise-figure AlGaAs/GaAs high electron mobility transistors. In 1985, he joined Hewlett-Packard Laboratories, Palo Alto, CA, investigating AlGaAs/GaAs HBT device physics, reliability, and circuit modeling. His work contributed to the development and application of HBT circuits in Hewlett-Packard wireless and optical communications instrumentation and component products. Since 1993, he has been managing a group in Hewlett-Packard Laboratories (now Agilent Laboratories) that has made contributions in InGaP/GaAs and InP HBT device technology; HBT device modeling; microwave, millimeter-wave, and gigabit HBT and HEMT integrated circuits; and signal-processing techniques for wireless and optical communications components and test instruments. He has participated in the IEDM Technical Subcommittee on Quantum and Compound Semiconductor Devices.

Dr. Camnitz is a member of the IEEE Electronic Device Society. He received the NSF and IBM Graduate fellowships.

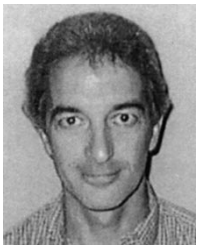

Donald C. D'Avanzo (S'72–M'78) received the B.S. degree in biomedical engineering from Brown University, Providence, RI, in 1973 and the M.S. and Ph.D. degrees in electrical engineering from Stanford University, Stanford, CA, in 1974 and 1980, respectively.

His thesis research included characterization and modeling of VMOS and DMOS transistors and spreading resistance measurements development and data analysis. Since 1979, he has been with the Microwave Technology Center, Agilent Technologies (formerly Hewlett-Packard), Santa Rosa, CA, initially as a Member of Technical Staff. Since 1982, he has been R&D Project Manager, responsible for the development of new GaAs IC technologies including MESFETs, PHEMTs, HBTs and diodes. He is the author or coauthor of numerous publications, presentations, and patents in the field of GaAs IC technology. He has served on the technical program committees of the GaAs IC Symposium, the International Microwave Symposium, and the Topical Workshop on Hetero-Junction Microelectronics.

Dr. D'Avanzo is a member of Tau Beta Pi, Sigma Xi, and the Electrochemical Society. He has served as the Symposium Chairman of the IEEE GaAs IC Symposium and the Electrochemical Society State of the Art Symposium on Compound Semiconductors.